ICAM 2009

Nanoscopic study of chemical species during uranium electrodeposition for alpha spectrometry sources

C. G. Méndez · H. E. Esparza-Ponce · A. M. Beesley · M. T. Crespo · L. Fuentes · L. Fuentes-Montero · G. Murillo · A. Varela · M. E. Montero-Cabrera

Abstract High resolution alpha spectrometry (AS) is commonly applied for the determination of actinides and other alpha-emitting nuclides in many applications. Electrodeposition is the standard procedure for preparing α-particle sources usually made of a thin and uniform radioactive deposit onto a metallic substrate. Natural U sources prepared by the Hallstadius method are known to contain co-deposited Pt from the anode. In this sense, the main aim of this work is to conclusively review the behaviour of Pt and U in the electrodeposition process and their distribution in the resulting deposit, factors that are responsible for the thickness and uniformity of the sources. In addition to new scanning electron microscopy/energy dispersive spectroscopy (SEM–EDX) and X-ray absorption fine structure (XAFS) data, the electrodeposited surface has been analyzed using both atomic force microscopy (AFM) and synchrotron radiation Grazing Incidence X-ray diffraction (GI-XRD). The results concerning morphology of the deposit, surface roughness, topography and surface structure obtained from sources prepared at different electrodeposition times agree with the AS results concerning electrodeposition yield and spectral resolution.

C. G. Méndez · H. E. Esparza-Ponce · L. Fuentes · L. Fuentes-Montero · M. E. Montero-Cabrera (✉)
Laboratorio Nacional de Nanotecnología, Centro de Investigación en Materiales Avanzados (CIMAV), Miguel de Cervantes 120, Compl. Industrial Chihuahua, 31109 Chihuahua, Mexico
e-mail: elena.montero@cimav.edu.mx

C. G. Méndez
e-mail: carmen.mendez@cimav.edu.mx

H. E. Esparza-Ponce
e-mail: hilda.esparza@cimav.edu.mx

L. Fuentes
e-mail: luis.fuentes@cimav.edu.mx

A. M. Beesley
School of Chemical Engineering and Analytical Science, The University of Manchester, Sackville Street, Manchester M60 1QD, UK
e-mail: Beesley.angela@gmail.com

M. T. Crespo
CIEMAT, LMRI, Avda. Complutense, 22, 28040 Madrid, Spain
e-mail: teresa.crespo@ciemat.es

G. Murillo · A. Varela
Departamento del Acelerador Tandem, Instituto Nacional de Investigaciones Nucleares (ININ), Carretera México-Toluca s/n, La Marquesa, 52750 Ocoyoacac, Mexico
e-mail: ghiraldo.murillo@inin.gob.mx

A. Varela
e-mail: armando.varela@inin.gob.mx

Abbreviations

AFM	Atomic force microscopy
AFM SPM MultiMode	Atomic force microscopy scanning probe microscope MultiMode system
AS	High resolution alpha spectrometry
CIEMAT, LMRI	Centro de Investigaciones Energéticas, Medioambientales y Tecnológicas, Laboratorio de Metrología de Radiaciones Ionizantes, España. In English: Center for Energy, Environmental and Technological Research, Laboratory for Metrology of Ionizing Radiation, Spain

CIMAV	Centro de Investigación en Materiales Avanzados, México. In English: Advanced Materials Research Center, Mexico
Fit-2D	General purpose and specialist 1 and 2 dimensional data analysis program
FWHM	Full width at half maximum of a spectroscopy peak, giving the resolution
GeV	Giga electron volt, energy unit
GI-XRD	Synchrotron radiation Grazing Incidence X-ray diffraction
HPS Inc	High purity standards Inc
ICSD	Inorganic crystal structure database
IFEFFIT	It is a library and set of interactive programs for the analysis of XAFS data
ININ	Instituto Nacional de Investigaciones Nucleares, México. In English: National Institute for Nuclear Research, Mexico
JEOL JSM-5800 LV	Japan Electron Optics Laboratory electron microscope, Model JSM-5800 Low Vacuum
PIPS detector	Passivated implanted planar silicon detector
Pt	Platinum
SD	Standard deviation
SEM-EDX or SEM-EDS	Scanning electron microscopy/energy dispersive X-ray spectroscopy
SPEAR-3	Stanford positron electron accelerating ring, storage ring of the SSRL synchrotron
SSRL	Stanford synchrotron radiation lightsource
U	Uranium
UL_3-edge	L_3-X-ray absorption edge of Uranium
UNAM	Universidad Nacional Autónoma de México. In English: National Autonomous University of Mexico
XAFS	X-ray absorption fine structure
XANES	X-ray absorption near edge spectroscopy
XPS	X-ray photoelectron spectroscopy
Y K edge	K X-ray absorption edge of Yttrium

Introduction

Alpha spectrometry (AS) is extensively used in a large number of applications such as nuclear decay data measurements [1], standardization of radionuclides [2], environmental [3, 4], geological [5], nuclear wastes characterization [6] and health studies [7, 8]. To produce accurate measurements, thin and uniform sources have to be prepared [9, 10] by electrodeposition which is the technique mostly used for source preparation [11]. Alpha sources produced by electrodeposition consist of a radioactive deposit onto a metallic substrate (cathode of the electrolytic cell) [12] where the presence of co-deposited platinum has been demonstrated [13–16] and believed to be originated from the dissolution of the anode during the electrodeposition. As early as 1905, Tafel and Emmert [17] described that platinum anodes were dissolved in sulphuric acid solutions. This feature, later demonstrated by [18] and more recently by [16], has not been taken into account properly in papers related to electrodeposition of actinides in the presence of sulphate ions. This is an important fact since many of the most popular methods of electrodeposition [12, 19, 20] include sulphate ions as components of the aqueous electrolyte.

In a recent paper by Beesley et al. [16], the morphology and composition of natural uranium sources prepared by the Hallstadius method, with co-deposited platinum were studied by scanning electron microscopy/energy dispersive spectroscopy (SEM–EDX), X-ray photoelectron spectroscopy (XPS) and X-ray absorption fine structure (XAFS). The role of porous platinum in the precipitation of oxyhydroxides of uranium, the evolution of the precipitate from reduced species towards aged oxidized crusts and its subsequent effect on the morphology of the sources and energy resolution of AS spectra were reported in [16]. However, no conclusive information concerning the phase identification of uranium deposits, thickness and homogeneity of the uranium deposits were presented. The last two factors are the most relevant from the practical point of view as they are associated to the long half-life of radionuclides that can in turn affect the high-energy resolution alpha spectra achieved with these sources.

To overcome these deficiencies, the aim of the present work is to conclusively review the behaviour of Pt and U in

the electrodeposition process and their distribution in the resulting deposit, factors that are responsible for the thickness and uniformity of the sources. To achieve this, in addition to new SEM–EDX and XAFS data, the surface of the deposit has been studied using both atomic force microscopy (AFM) and synchrotron radiation grazing incidence X-ray diffraction (GI-XRD). The results concerning morphology of the deposit, surface roughness and topography and surface phase identification obtained from sources prepared at different electrodeposition times are in good agreement with AS results concerning electrodeposition yield and spectral resolution.

Experimental

All sources were prepared by the Hallstadius [19] method from a sulphuric acid electrolyte at pH 2.1–2.4, with Na_2SO_4 to prevent adsorption onto the walls of the electrodeposition cells. Deposition was carried out onto mirror polished stainless steel (SS) discs (2.5 cm diameter, 2.2 cm diameter of active area, 1 mm thickness) acting as cathode and a 1 mm diameter Pt wire folded into a spiral base shape of 15 mm diameter acting as anode. Current densities of 0.52 A cm^{-2} and 7 mm distance between electrodes were used.

Six sets of sources were studied in this paper, the uranium content and studies performed over them are summarized in Table 1. Two sets were studied in Beesley et al. [16] (CIEMAT-1 and 2 in Table 1), these sources were prepared at CIEMAT from a natural uranium standard solution of 6.15 ± 0.15 Bq/g activity concentration in 1 M HNO_3. The other four sets of sources were prepared at CIMAV. Each set consists of three sources obtained at electrodeposition times of 20, 40 and 60 min. One set was prepared in the absence of uranium salt in the electrolyte (CIMAV-Blank in Table 1). Another set (CIMAV-Unat in Table 1) was prepared by adding 150 μL of a HPS Inc. natural uranium standard solution of 1,000 μg/mL ± 3% concentration to the electrolyte solution [21]. The last two sets (CIMAV-UAc-1 and CIMAV-UAc-2) were prepared by adding 157 μL of uranyl acetate solution of 13.65 ± 6% Bq/mL (Polyscience Inc., containing depleted uranium, activity ratio U-234/U-238 = 0.156 ± 0.008 [22]) dissolved in acetic acid at pH 4 to the sulphuric electrolyte. All electrodeposition experiments for the same set of samples were performed with the same initial quantity of uranium. In consequence, for CIEMAT-1 and 2, the electrodeposition yield is about 100% for the 60 min electrodeposition time sources and decreases to about 77% when the time decreases. These values are lower than those found by Vera Tomé and Martin Sánchez [23] for ^{232}U sources and can be explained by the important differences in mass when using ^{232}U instead of natural uranium. For 60 min electrodeposition the recovery is proved to be 100% [23]. For CIMAV-Unat, CIMAV-UAc-1 and

Table 1 Set of prepared sources, included in the present study

Sample	Uranium mass (μg)	Set	Studies performed over samples reported in the present work
U15-20	128	CIEMAT-1	SEM/EDX (CIMAV), AFM (CIMAV)
U5-40	131		
U14-60	153		
U12-20	128	CIEMAT-2	
U4-30	120		
U13-40	134		
U17-60	155		
Blank-20	–	CIMAV-Blank	SEM/EDX (CIMAV), AFM (CIMAV)
Blank-40	–		
Blank-60	–		
Unat-20	112	CIMAV-Unat	SEM/EDX (CIMAV), AS (ININ)
Unat-40	89		
Unat-60	121		
UAc-20	107	CIMAV-UAc-1	SEM/EDX (CIMAV), XAFS (SSRL), GI-XRD (SSRL), AS (ININ)
UAc-40	85		
UAc-60	116		
UAc(2)-20	110	CIMAV-UAc-2	SEM/EDX (CIMAV)
UAc(2)-40	90		
UAc(2)-60	120		

CIMAV-UAc-2 sets, the yield varies in the range 80–57%, being always the highest values for the 60 min electrode-position times.

Alpha spectrometry (AS) was recorded at ININ on the sets of samples CIMAV-Unat and CIMAV-UAc-1 with a 100 mm^2 PIPS detector lodged in a CANBERRA 7401 alpha spectrometer and a source-to-detector distance of 10 mm. The counting time was set to 24 h which allowed recording of spectral resolution for the three CIMAV-Unat sources.

The morphology of the sources was studied at CIMAV, using a scanning electron microscope JEOL JSM-5800 LV coupled to an EDX. AFM experiments on the CIMAV-Blank and CIEMAT-2 sources were performed at CIMAV with a SPM MultiMode using a NanoScope IVa controller [24] in tapping mode. Si (n-type, doped with Sb) tip cantilevers with a force constant of 20–80 N m^{-1}, a 110–140 μm length and a resonance frequency of 300 kHz were used. The sources were cut in two parts to obtain topographical images from different sections as represented in Fig. 1. Analysis was carried out over five different points at each zone in order to measure average roughness values (Fig. 1). Digital Instruments Nanoscope 5.30r3sr3 software was used for AFM image recording and analysis. Roughness was calculated as the root mean square of different point heights within the area under study.

XAFS at the UL$_3$-edge were taken on CIMAV-UAc-1 sources at the Stanford Synchrotron Radiation Lightsource (SSRL) beamline 2–3. The SPEAR-3 storage ring was operated at 3.0 GeV with a beam current of 100 mA. We used a Si(220) double crystal monochromator, $\varphi = 0$. The beam size was 1.0 mm × 10.0 mm. XAFS U L$_3$ spectra were acquired in total electron yield mode using the collector current. Data were recorded on an energy grid of 10 eV/step in the pre-edge region and 0.35 eV/step in the remaining X-ray absorption near edge spectra (XANES)
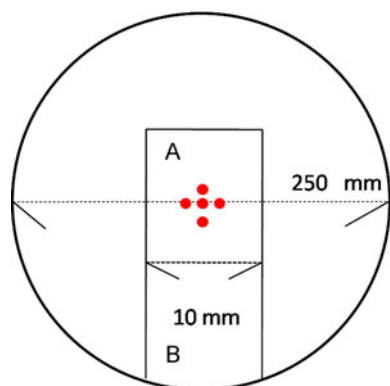
region, with an integration time of 1 s/step. An energy calibration of the beam was performed by collecting the transmission spectra of a reference Y foil at the Y K edge. A total of six scans were obtained for each source. Spectra obtained from sources prepared with the same electrode-position time were averaged. Athena software (IFEFFIT front-end) was used for alignment of XAFS spectra [25].

Synchrotron radiation Grazing Incidence X-ray diffraction (GI-XRD) patterns were obtained at SSRL, at beamline 11–3 [26, 27]. The experimental setup and calibration conditions used in the detection were as follows: 2D-detector diameter = 345 mm; pixel size = 0.1 mm; X-ray spot size = 0.1 mm 2D position-sensitive detector calibrated with a LaB$_6$ standard sample; sample detector distance = 150 mm; incidence angle = $(0.5 \pm 0.5)°$; X-ray wavelength $\lambda = 0.97354$ Å; Experimental 2D patterns were processed by means of Fit-2D software [28].

Results

Alpha spectrometry

AS spectra for CIMAV-Unat sources are presented in Fig. 2, the inset corresponds to the FWHM U-234 peak. This result confirms the worsening of spectral resolution as electrodeposition time increases during source preparation.

SEM/EDX studies

Figure 3 shows the morphology of CIMAV-UAc-2 uranium sources for which EDX elemental analysis are shown in Table 2. SEM images of the sources confirm the
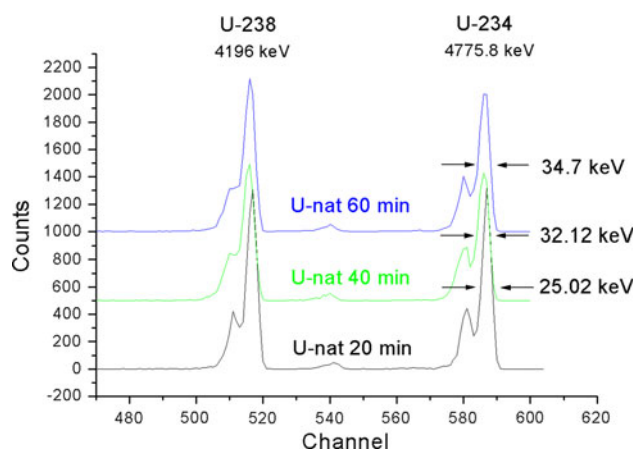
Fig. 1 Schematic representation of the sections across CIEMAT-2, CIMAV-blank and CIMAV-UAc-2 sources studied using AFM. Point A corresponds to the central zone and B to the out-of-centre zone

Fig. 2 Alpha spectra of natural uranium sources, showing the FWHM for the 4775.8 keV peak. The decrease in resolution as electrodeposition time increases is easily observed on the U-238 doublet which turns into a shoulder for greater electrodeposition times. Spectra are vertically shifted for clarity
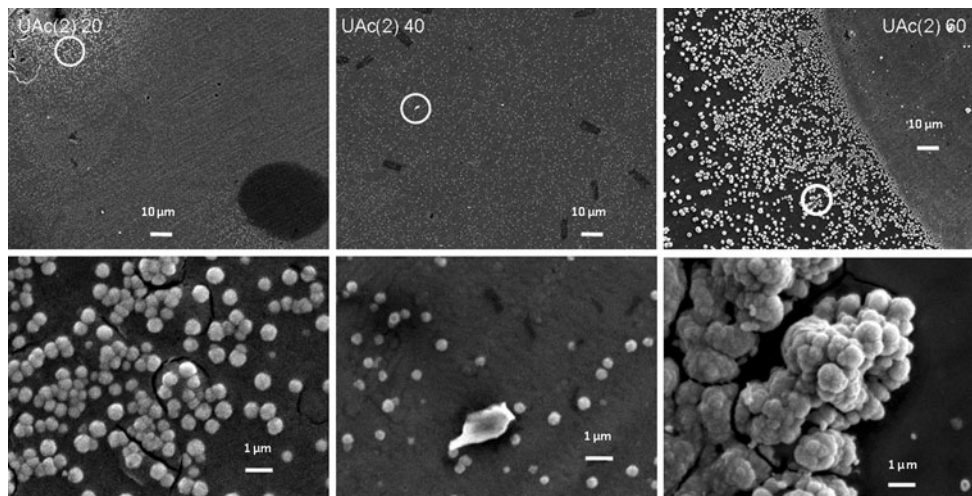
Fig. 3 *Top* morphology obtained by SEM of CIMAV-UAc-2 sources at magnification ×1,200. *Bottom* images obtained at magnification ×15,000 at zones *circled* in the top images

Table 2 Semi quantitative EDX elemental analysis in at.%, taken on CIMAV-UAc-2 set

Element	UAc-20	UAc-40	UAc-60
C	22.32	21.91	22.12
O	12.94	12.06	12.50
Si	1.07	0.74	0.91
Cr	12.38	12.77	12.57
Mn	0.74	0.69	0.71
Fe	42.30	40.48	41.39
Ni	4.58	4.64	4.61
Pt	2.17	4.92	3.54
U	1.51	1.82	1.66

Relative errors are considered to be less than 1%

spherulitic structure described by Weber et al. [15] as well as spheres with <1 μm diameter. The spherules have a diameter of ∼400 nm for the 20 min source, whereas for the 60 min uranium source SEM images show the evolution of individual spheres towards colloidal-like agglomerates, similar to those described in [16]. These are believed to correspond to the previous morphological step before aged crusts are formed, as explained in the next sections. From the analysis it can also be observed that uranium sources follow the same trend as the platinum in the blanks (see Fig. 1 from [16]), i.e. from individual spheres to a final agglomerate-type. EDX analysis of uranium sources show that the weight ratio Pt/U is very similar for all three sources and follow the same trend as those found in CIEMAT sources [16] of Pt/U > 1. These data confirm the role played by platinum in the deposition of uranium given that U precipitation seems to occur preferentially at those points on the surface containing precipitated platinum dissolved from the anode.

AFM measurements

AFM results are shown in Figs. 4 and 5, for both the central zone (A) and the out-of-centre (B) zone (Fig. 1). Figure 4 shows some AFM images obtained from zone A of CIMAV-Blank and CIEMAT-2 sources prepared at electrodeposition times of 20, 40 and 60 min. From Fig. 4 it is observed a clear increase in surface roughness of the sources deposited at longer times. Analysis of the AFM data at different points on the deposit space allowed the determination of zones with higher homogeneity.

Figure 5 presents roughness values [mean and standard deviation (SD)] calculated over five different points within the central zone and out-of-centre zone for CIMAV-Blank set and CIEMAT-2 sources. From the figure it is clear that the deposit is more homogeneous at the centre of the source and that large variation on roughness mean and SD are present at the out-of-centre zones. A possible explanation of this effect is that the centre of the deposit is located directly below the Pt electrode in the electrodeposition cell. At this point higher and more uniform current density is achieved during deposition which in turn gives rise to a more uniform platinum + uranium deposit. The trend of increasing mean and SD values from sources electrodeposited from 20 to 60 min (Fig. 5) supports the relationship between source heterogeneity and decrease in resolution observed by AS, both in Fig. 2 and in [16] particularly in the case of the out-of-centre (B) zone of the deposit.

XANES study of oxidation state of samples

Figure 6 shows the comparison of XANES spectra from CIMAV-UAc-1 sources with UO_2 (with U^{4+}) and becquerelite (uranyl mineral with U^{6+}) spectra, measured in
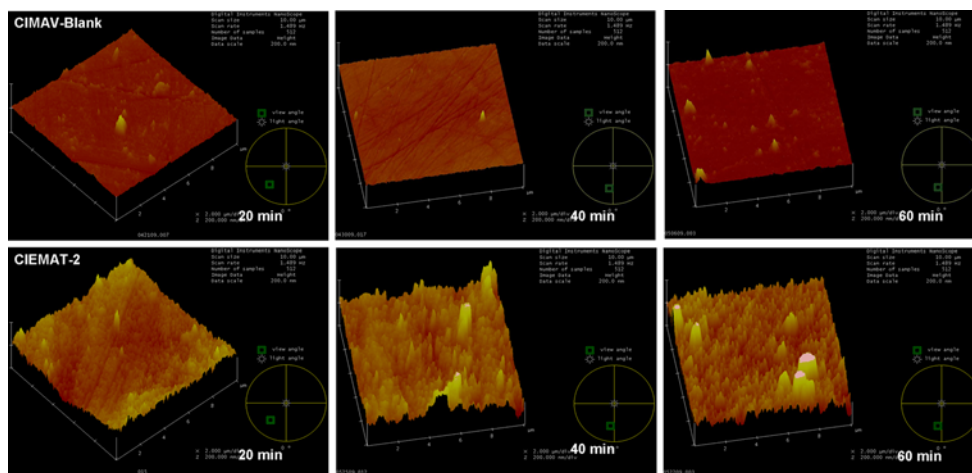
Fig. 4 AFM images of some points at the central zone of the sources sets CIMAV-Blank and CIEMAT-2. *X* and *Y* dimensions are both 10 μm, whereas *Z*-scale is 200 nm. In both *X* and *Y* directions a total of 512 points were scanned, resulting in 262144 points for the R_{rms} calculation
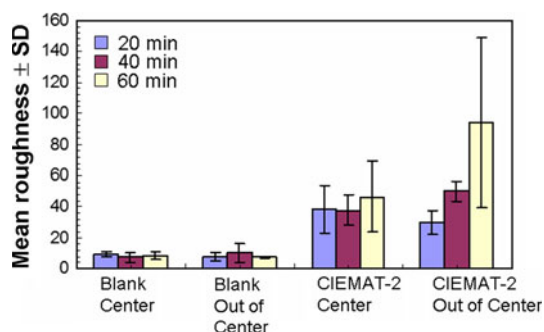

Fig. 5 Roughness mean and standard deviation (SD) values calculated over five different points for CIMAV-Blank set and CIEMAT-2 sources

similar conditions as reference compounds at SSRL. Feature A is the maximum at resonance ('white line'), which is broader in uranyl compounds; feature B is characteristic of uranyl species and feature C accounts for the backscattering of the photoelectron by the second sphere neighbours [29].

We may observe that all CIMAV-UAc-1 sources show a broad white line peak characteristic of the uranyl ion structure. Sources prepared by 20 min electrodeposition showed a shift in energy. As discussed in [16], different uranium oxidation states produce UL_3 edge shifts towards higher energies in the order UO_2, U_3O_8, UO_3 due to reduced shielding of the core electrons associated with an increase in mean valence state across the oxidation series [30–34]. Figure 6 shows the position of the absorption edge in the XANES spectra. The inset indicates the relative position of the white line of uranium species in the sources in relation to the extreme oxidation states +4 and +6. Based on reported values cited above and on the measured reference compounds, UAc-60 corresponds to a mixture of U(IV) and U(V), whereas UAc-20 and UAc-40 correspond
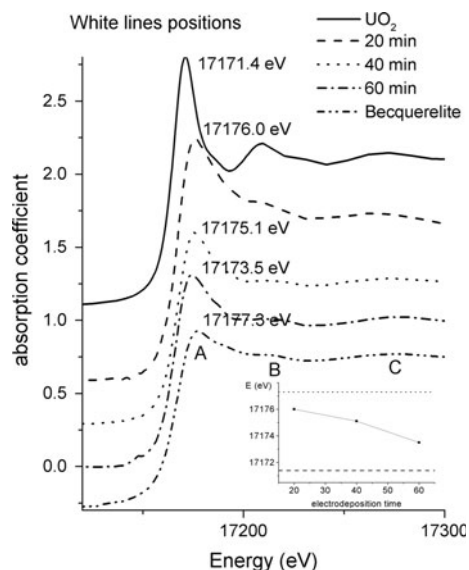

Fig. 6 XANES spectra of the UL_3-edge of CIMAV-UAc-1 sources and reference compounds: UO_2 and becquerelite synthetic mineral. The inset shows the energy positions of white lines for CIMAV-UAc-1 sources, given by the electrodeposition time relative to U(IV) *white line* position (*dashed at bottom*) and to U(VI) position (*top dots*). Spectra are vertically shifted for clarity

to a mixture of U(V) and U(VI), with UAc-20 closer to U(VI). All these features are in agreement with the results presented in [16].

X-ray scattering from grazing incidence on uranium sources

GI-XRD on sources set CIMAV-UAc-1 was performed with different incidence angles, from $\varphi = 0.0$ to $0.8°$. Figure 7 shows part of the measured 2D patterns. The 2D patterns were integrated by azimuthal angle to produce the
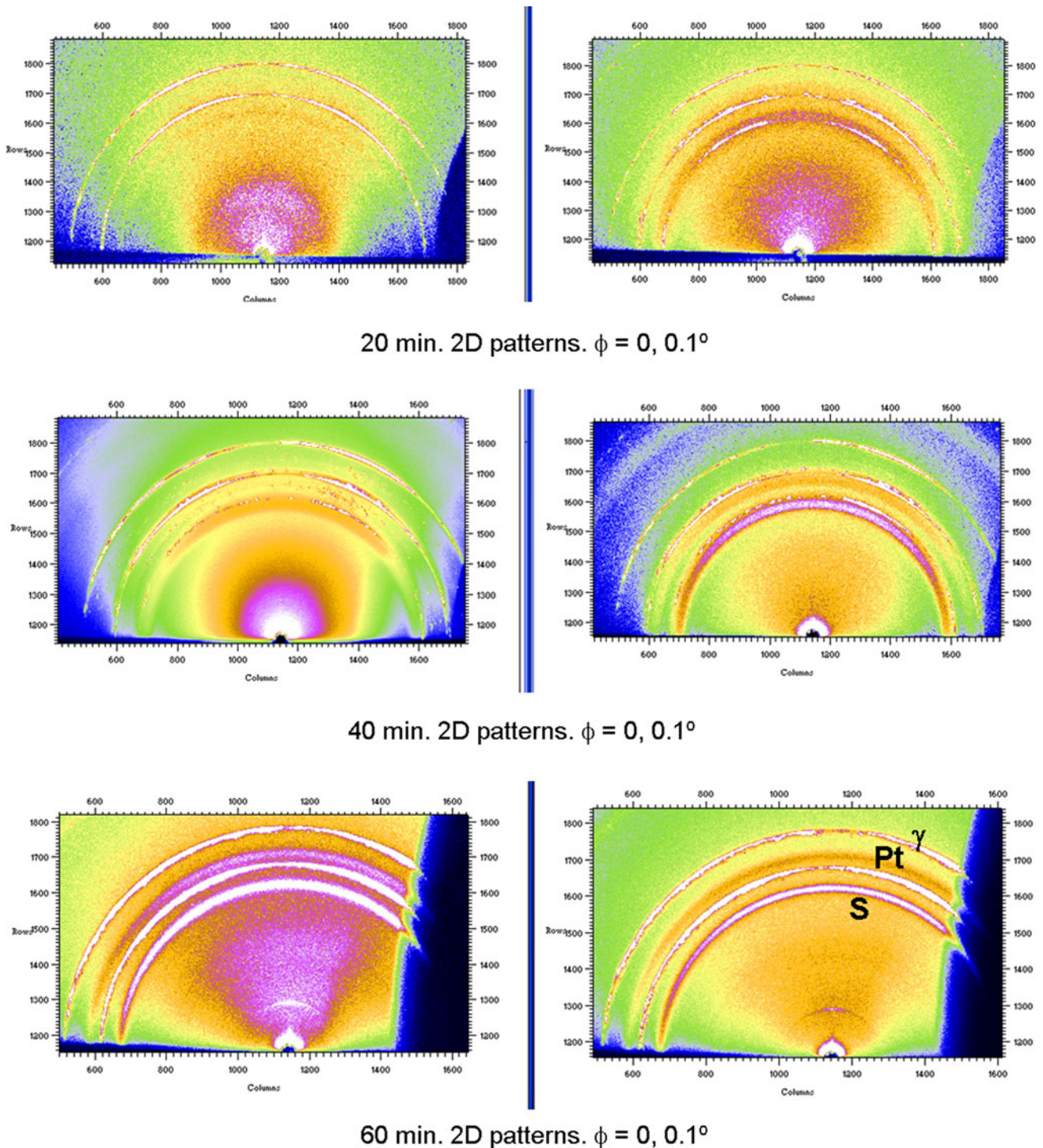
20 min. 2D patterns. φ = 0, 0.1°

40 min. 2D patterns. φ = 0, 0.1°

60 min. 2D patterns. φ = 0, 0.1°

Fig. 7 2D XRD patterns of samples obtained with different electrodeposition times (CIMAV-UAc-1 sources). Characteristic Debye rings from steel (γ), Pt and schoepite (S) are identified in the 60 min sample

1D patterns shown in Figs. 8 and 9. From the analysis of these 1D patterns, different compounds were identified and information on crystallographic phases was also obtained. Phase identification was carried out based on ICSD database [35]. For the elucidation of the uranium compounds

present in the analyzed sources, several options were considered. The broad peaks in the low 2θ zone can be associated to uranium compounds of large reticular parameters. The best candidate for the uranium phase was uranium oxyhydroxide known as schoepite. Figure 9 shows
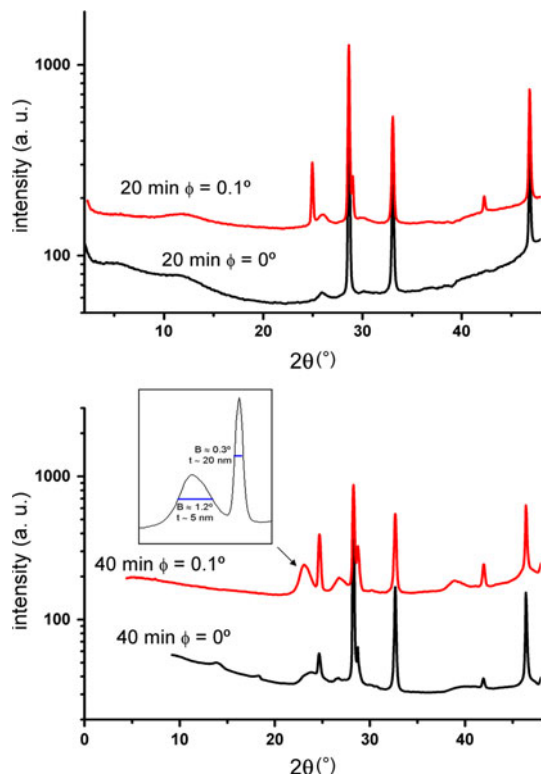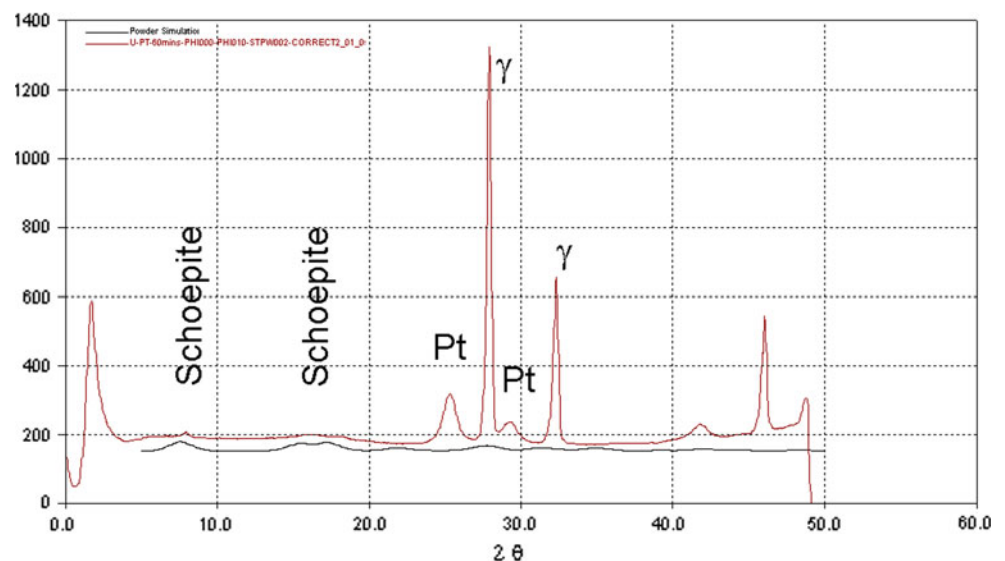
Fig. 8 1D XRD patterns corresponding to 2D diagrams shown in Fig. 6, for sources UAc-20 and UAc-40. Sharp peaks correspond to the SS substrate (basically, Ni–Cr solid solution in γ-Fe). Broad humps on the low-angle interval may be attributed to nanostructured schoepite. Patterns are vertically shifted for clarity

the computer-modelled diagram of a 1D pattern of UAc-60 source. The broad Pt peaks are located either on the left, below or on the right of the sharp Pt peaks, depending on the location of the nanocrystals on the deposited source. The peaks attributed to schoepite in the 60 min 1D pattern, may have different locations in other patterns hence the

schoepite identification is not univocal. Analyzing the profile of broad peaks from Pt and schoepite phases and applying the Scherrer equation [36], crystallite dimensions of these phases were estimated. Pt peaks present crystallite sizes of $t \sim 20$ nm and ~ 5 nm and schoepite diffraction signals indicate poorly crystallized grains ($t < 5$ nm).

In Fig. 7, heterogeneous intensity distribution along steel Debye rings reveals this phase has a rolling texture [37]. Pt does not show any texture. Split-broadened peaks in Fig. 8 are produced by bi-modal size distribution of Pt grains. Dispersion in the location of the broadened Pt peaks is produced by heterogeneity in the distribution of Pt nanoparticles on the source surface. This feature was observed and confirmed in all the GI-XRD patterns recorded for each CIMAV Ac sources.

The whole analysis of GI-XRD can be summarized as follows: (1) the spectra indicates a bi-modal presence of Pt where there is a well crystallized Pt layer, consequence of some *old* Pt deposit and registered as sharp peaks. In addition, there is a *new* nanocrystalized Pt that appears on apparently isolated places on the surface of the deposit associated to the broad Pt peaks in GI-XRD patterns located around the Pt sharp peaks. These *new* Pt tends to grow or even coalesce as it becomes *aged* Pt. (2) Deposited uranium forms poorly crystallized layers associated to schoepite, with crystal sizes of approximately 5 nm and layer thickness of 50 nm on average (this figure is given based on the amount of electrodeposited uranium on the deposit area).

Conclusions

SEM/EDX data obtained from sources prepared by elec-trodeposition of uranyl acetate (depleted uranium) show

Fig. 9 1D diffractogram obtained by azimuthal integration of a representative 2D pattern from the source UAc-60. For this sample, patterns collected with different incidence angles were practically coincident. Peaks produced by characteristic phases are identified. The weak pattern in the lower part is a computer-modelled diagram corresponding to nanocrystalline schoepite

the same trend previously reported in [16]. These data confirm the synergistic behaviour of platinum and uranium in the electrodeposition based on sulphuric electrolytes, given that uranium precipitation seems to occur preferentially on clusters of precipitated platinum dissolved from the anode.

Calculated AFM roughness results suggest that the non-homogeneous surface points act as nucleation points for further deposits and hence are responsible for thickness increase, leading to loss of resolution observed by AS both in Fig. 2 and in [16].

XANES results suggest that the electrodeposition carried out for short periods (20 min) produce more oxidized precipitates than those undertaken for extended periods. This result is not trivial, since one of the differences between the XAFS experiment discussed in [16] and the one presented in this paper is that in the latter, the sources were prepared very shortly before the XANES study. Another point of interest is that in both cases the sources were kept in an aerobic environment at all times. Surprisingly, reduced species of uranium present in UAc-60 were not oxidized in air. All these features are in agreement with the results presented in [16].

The GI-XRD results complete the picture presented by the techniques discussed previously. Metallic platinum (or a solution of Pt and U hardly distinguishable from pure Pt) is detected simultaneously well and poorly crystallized. The location of the broad peaks associated to the nanometric *new* platinum appears in several patterns at different sides of the sharp Pt peaks (from *old* well crystallized Pt). This phenomenon has been attributed [38] to the isolated location of nanosized clusters on the sample, resulting in the dispersion of the sample–detector distance.

Deposited uranium forms poorly crystallized layers probably of schoepite, with crystal size of approximately 5 nm. Detection of schoepite (uranyl oxihydroxide) is consistent with the Hansen theory and confirms the conclusion given in [16] about predominance of uranyl-type structures with pentagonal bipyramids.

At short electrodeposition times, i.e. 20 min the free energy surface of U–Pt particles does not favour agglomeration and therefore particles are kept isolated. After 40 min of electrodeposition almost all available uranium is deposited on a homogeneous layer. At a longer electrodeposition times (60 min) platinum is deposited again increasing the roughness and size of agglomerates.

References

1. Pommé S, García-Toraño E, Sibbens G, Richter S, Wellum R, Stolarz A, Alonso A (2008) J Radioanal Nucl Chem 277:207
2. Crespo MT (2007) Appl Radiat Isot 65:897
3. Al-Kharouf SJ, Al-Hamarneh IF, Dababneh M (2008) J Environ Radioact 99:1192
4. Hurtado S, Jiménez-Ramos MC, Villa M, Vioque I, Manjón G, García-Tenorio R (2008) Appl Radiat Isot 66:808
5. Bonotto DM, Bueno TO (2008) Appl Radiat Isot 66:1507
6. Quejido AJ, Perez del Villar L, Cozar JS, Fernandez-Diaz M, Crespo MT (2005) Appl Geochem 20:487
7. Manickam E, Sdraulig S, Tinker RA (2008) J Environ Radioact 99:491
8. Maxwell SL III, Jones VD (2009) Talanta 80:143
9. Martín Sánchez A, Jurado Vargas M, Nuevo Sánchez MJ, Fernández Timón A (2008) Appl Radiat Isot 66:804
10. Vera Tomé F, Jurado Vargas M, Martin Sánchez A (1994) Nucl Instr Meth A 348:183
11. Garcia-Torano E (2006) Appl Radiat Isot 64:1273
12. Talvitie NA (1972) Anal Chem 44:280
13. Ferrero Calabuig JL, Martin Sanchez A, Roldan Garcia C, Rosello Ferrando J, Da Silva MF, Soares JC, Vera Tome F (1996) Nucl Instr Meth A 369:603
14. Ferrero Calabuig JL, Vera Tome F, Martin Sanchez A, Roldan Garcia C, Da Silva MF, Soares JC, Ager FJ, Juanes Barber D, Rubio Montero P (1998) Nucl Instr Meth B 136–138:290
15. Weber R, Vater P, Esterlund RA, Patzelt P (1999) Nucl Instr Meth A 423:468
16. Beesley AM, Crespo MT, Weiher N, Tsapatsaris N, Cózar JS, Esparza H, Méndez CG, Hill P, Schroeder SLM, Montero-Cabrera ME (2009) Appl Radiat Isot 67:1559
17. Tafel J, Emmert B (1905) Z Physik Chem, Stoechiometrie und Verwandtschaftslehre 52:349
18. Ota KI, Nishigori S, Kamiya N (1988) J Electroanal Chem Interfacial Electrochem 257:205
19. Hallstadius L (1984) Nucl Instr Meth Phys Res 223:266
20. Mitchell RF (1960) Anal Chem 32:326
21. High-Purity Standards Inc (2009) Charleston, SC 29423
22. Polyscience Inc (2009) Warrington, PA 18976
23. Vera Tomé F, Martin Sánchez A (1991) Appl Radiat Isot 42:135
24. Veeco Instruments Inc (2005) SB, CA, USA. http://www.veeco.com/atomic-force-microscope-systems/index.aspx
25. Ravel B, Newville M (2005) J Synchrotron Radiat 12:537
26. Fuentes-Montero L, Montero-Cabrera ME, Calzada L, Pérez de la Rosa, Raymond O, Font R, García M, Torres M, Mehta A, Fuentes L (2008) Integr Ferroelectr 101:101
27. Stojanovic N (2009) Experimental station 11-3, SSRL, (Stanford Synchrotron Radiation Lightsource)
28. Hammersley AP (2004) FIT2D V12. 012 Reference Manual V6. 0, in "ESRF International Report No. ESRF98HA01T. Program available at http://www.esrf.eu/computing/scientific/FIT2D"
29. Den Auwer C, Drot R, Simoni E, Conradson SD, Gailhanou M, Mustre de Leon J (2003) New J Chem 27:648
30. Duff MC, Amrhein C, Bertsch PM, Hunter DB (1997) Geochim Cosmochim Acta 61:73

31. Jernstrom J, Eriksson M, Osan J, Tamborini G, Torok S, Simon R, Falkenberg G, Alsecz A, Betti M (2004) J Anal At Spectrom 19:1428

32. Salbu B, Janssens K, Lind OC, Proost K, Gijsels L, Danesi PR (2005) J Environ Radioact 78:125

33. Denecke MA (2006) Coord Chem Rev 250:730

34. Soldatov AV, Lamoen D, Konstantinovic MJ, Van den Berghe S, Scheinost AC, Verwerft M (2007) J Solid State Chem 180:54

35. Allmann R, Hinek R, Bergerhoff G, Brown ID (2009) ICSD—inorganic crystal structure database. National Institute of Standards and Technology (NIST), FIZ Karlsruhe

36. Smilgies DM (2009) J Appl Crystallogr 42:1030

37. Cullity BD, Stock SR (2001) Elements of X-ray diffraction. Prentice Hall, Upper Saddle River, NJ

38. Torres Sancho M (2009) Study of ferroelectric PbTiO₃ nanostructures deposited onto substrates and prepared by a novel microemulsion mediated synthesis. PhD Thesis, "Instituto de Química y Materiales Alvaro Alonso Barba" (Universidad Carlos III de Madrid, Leganés, Madrid), p 172